The underlying physical meaning of the $v_{\rm max} - v_{\rm c}$ relation

K. Belkacem^{1,2}, M.J. Goupil³, M.A. Dupret², R. Samadi³, F. Baudin¹, A. Noels², and B. Mosser³

- ¹ Institut d'Astrophysique Spatiale, CNRS, Université Paris XI, 91405 Orsay Cedex, France
- ² Institut d'Astrophysique et de Géophysique, Université de Liège, Allée du 6 Août 17-B 4000 Liège, Belgium
- ³ LESIA, UMR8109, Université Pierre et Marie Curie, Université Denis Diderot, Obs. de Paris, 92195 Meudon Cedex, France

July 26, 2018

ABSTRACT

Asteroseismology of stars that exhibit solar-like oscillations are enjoying a growing interest with the wealth of observational results obtained with the CoRoT and Kepler missions. In this framework, scaling laws between asteroseismic quantities and stellar parameters are becoming essential tools to study a rich variety of stars. However, the physical underlying mechanisms of those scaling laws are still poorly known. Our objective is to provide a theoretical basis for the scaling between the frequency of the maximum in the power spectrum (ν_{max}) of solar-like oscillations and the cut-off frequency (ν_c). Using the SoHO GOLF observations together with theoretical considerations, we first confirm that the maximum of the height in oscillation power spectrum is determined by the so-called *plateau* of the damping rates. The physical origin of the plateau can be traced to the destabilizing effect of the Lagrangian perturbation of entropy in the upper-most layers which becomes important when the modal period and the local thermal relaxation time-scale are comparable. Based on this analysis, we then find a linear relation between ν_{max} and ν_c , with a coefficient that depends on the ratio of the Mach number of the exciting turbulence to the third power to the mixing-length parameter.

Key words. Convection - Turbulence - Stars: oscillations - Stars: interiors

1. Introduction

Scaling relations between asteroseismic quantities and stellar parameters such as stellar mass, radius, effective temperature and luminosity have been observationally derived by several authors (e.g. Kjeldsen & Bedding 1995; Chaplin et al. 2008, 2009; Stello et al. 2009a) using ground-based data. More recently, the space-missions CoRoT and Kepler confirmed those results by providing accurate and homogeneous measurements for a large sample of stars from red giants to main-sequence stars (e.g., Mosser et al. 2010). Scaling relations are essential to study a large set of stars (e.g., Kallinger et al. 2009; Stello et al. 2009b) for which, in general, little is known, to provide a first order estimate for mass and radius (e.g., Basu et al. 2010; Mosser et al. 2010), or to probe the populations of red giants (Miglio et al. 2009).

Scaling laws can also lead to a better understanding of the underlying physical mechanisms governing the energetical behaviour of modes. In particular, it has been conjectured by Brown et al. (1991) that the frequency of the maximum of the power spectrum ($\nu_{\rm max}$) scales as the cut-off frequency $\nu_{\rm c}$ because the latter corresponds to a typical time-scale of the atmosphere. The continuous increase of detected stars with solar-like oscillations has then confirmed this relation (e.g., Bedding & Kjeldsen 2003; Stello et al. 2009a). However, the underlying physical origin of this scaling relation is still poorly understood. Indeed, $\nu_{\rm max}$ is associated with the coupling between turbulent convection and oscillations and results from a balance between the damping and the driving of the modes. The cut-off frequency is associated with the mean surface properties of the star and the sound speed, making the origin of the $\nu_{\rm max}-\nu_{\rm c}$ relation very intriguing.

As a first step toward an understanding, one has to determine which of the damping rate or the excitation rate is the main responsible for the maximum of power in the observed spectra. Chaplin et al. (2008), using a theoretical approach, pointed out that in the solar case v_{max} coincides with the plateau of the linewidth variation with frequency. We will confirm this result using observations from the GOLF instrument in the solar case. However, several issues remain to be addressed: is ν_{max} for any star directly related with the observed plateau in the modewidths variation with frequency? In case of a positive answer, what is the origin of this relation? The first issue is quite difficult to answer as it is expected to strongly depend on the model used for the description of the pulsation-convection interaction. Nevertheless, CoRoT observations begin to answer this issue and several stars (HD49933, HD180420, HD49385, and HD52265) suggest that v_{max} correponds to the plateau of the damping rates (see Benomar et al. 2009; Barban et al. 2009; Deheuvels et al. 2010; Ballot et al. 2011, for details). The second step consists in determining the main physical causes responsible for the plateau of the damping rates and its mean frequency (ν_{Γ}) . Subsequently, one has to determine a general scaling law that relates the frequency of the plateau of the damping rates to the stellar parameters. In this paper, we discuss the first issue then we focus on the second issue by deriving a theoretical relation between ν_{Γ} and $\nu_{\rm c}$. If one accepts the positive answer to the first issue, this also provides the scaling relation between v_{max} and v_{c} .

This paper is organised as follows. In Sect. 2 we present the observed scaling law obtained from a homogeneous set of CoRoT data and show that the maximum mode height in the solar power spectrum coincides with a marked minimum of the mode-width when corrected from mode inertia. We then point out, in Sect. 3, that such a minimum is the result of a destabilizing effect in the super-adiabatic region. The relation between $\nu_{\rm T}$

and ν_c is demonstrated in Sect. 4, and conclusions are provided in Sect. 5.

2. The observed scaling law

We use the CoRoT seimological field data to ensure a homogeneous sample: HD49933 (Benomar et al. 2009), HD181420 (Barban et al. 2009), HD49385 (Deheuvels et al. 2010). We also use the results on HD50890 (Baudin et al. 2011) and on HD181907 (Carrier et al. 2010), a red giant, and the Sun. The characteristics of these stars are listed in Table 1, as well as the way their fundamental parameter is obtained.

For the Sun, due to the presence of pseudo-modes above the cut-off frequency (e.g. Garcia et al. 1998), observational determination of ν_c is not obvious. Nevertheless, one can infer a theoretical relation for this frequency $\omega_c = c_s/2H_\rho \propto g/\sqrt{T_{\rm eff}} \propto M\,R^{-2}\,T_{\rm eff}^{-1/2}$ (e.g., Balmforth & Gough 1990), where c_s is the sound speed, H_ρ the density scale height, g the gravitational field, M the mass, R the radius, and $T_{\rm eff}$ the temperature at the photosphere. When scaled to the solar case, this relations becomes

$$v_{\rm c} = v_{\rm co} \left(\frac{M}{M_{\odot}}\right) \left(\frac{R}{R_{\odot}}\right)^{-2} \left(\frac{T_{\rm eff}}{T_{\rm eff\odot}}\right)^{-1/2},\tag{1}$$

with $\nu_{\rm c\odot}=5.3 {\rm mHz}$, and $M_{\odot}, R_{\odot}, T_{\rm eff\odot}$ the solar values of mass, radius, and effective temperature respectively. Note that we will assume $H_{\rho}=H_{\rm p}=P/\rho g$ with P,ρ respectively denoting pressure, density. This is a commonly used approximation (e.g., Stello et al. 2009a) that presupposes an isothermal atmosphere, which is of sufficient accuracy for our purposes.

Using the stars listed in Table 1, and their measured ν_{max} , the relation between v_{max} and v_{c} is displayed in Fig. 1. It relies on two kinds of results: direct observations of v_{max} in the spectrum of the star on one hand, and on estimates of the mass (M), radius (R) and effective temperature (T_{eff}) of the star on the other hand. The latter are derived from photometric or spectroscopic observations but can be derived in some cases from stellar modelling. Here, M and R must be derived from stellar modelling and not from scaling laws as the aim of this work is to establish such a scaling law. The strict proportionality (the fitted slope is 1.01 ± 0.02) is clearly seen from this sample spanning from the Sun to a luminous red giant (HD50890). This is in agreement with the results obtained by several authors for main-sequence stars (e.g., Bedding & Kjeldsen 2003), as well as red giants (e.g. Mosser et al. 2010). The issue is now to assess the physical background underlying this relation.

3. Height maximum in the power spectrum

In this section, we confirm that the maximum of the power spectrum of solar-like oscillations is related to the plateau of the linewidth by using solar observations from the GOLF instrument and we then discuss the physical origin of the depression of the damping rates (i.e. the plateau).

Origin of the maximum of height in the power density spectrum

We consider the height H of a given mode in the power spectrum, which is a natural observable. To derive it, let us first define the damping rate of the modes given by (e.g., Dupret et al. 2009)

$$\eta = \frac{-W}{2\,\omega\,|\xi_r(R)|^2\mathcal{M}}\,,\tag{2}$$

Star name	T_{eff} (K)	M/M_{\odot}	R/R_{\odot}	$v_{\text{max}} (\mu \text{Hz})$
Sun	5780	1	1	3034
HD49933	6650	1.2	1.4	1800
HD181420	6580	1.4	1.6	1647
HD49385	6095	1.3	1.9	1022
HD52265	6115	1.2	1.3	2095
HD181907	4760	1.7	12.2	29.4
HD50890	4665	4.5	31	14

Table 1. Stellar characteristics (from the literature - see references in Sect 2) for the stars used in the comparison with the present results. For HD49933, $\nu_{\rm max}$ and $T_{\rm eff}$ are taken from Benomar et al. (2009); M and R are taken from Benomar et al. (2010). For HD181420, $\nu_{\rm max}$ and $T_{\rm eff}$ are taken from Barban et al. (2009); M and R are provided by M.-J. Goupil (private communication). For HD49385, $\nu_{\rm max}$ and $T_{\rm eff}$ are taken from Deheuvels et al. (2010); M and R are provided by M.-J. Goupil (private communication). For HD181907, $\nu_{\rm max}$ and $T_{\rm eff}$ are taken from Carrier et al. (2010). For HD50890, $\nu_{\rm max}$, $T_{\rm eff}$, M and R are taken from Baudin et al. (2011).

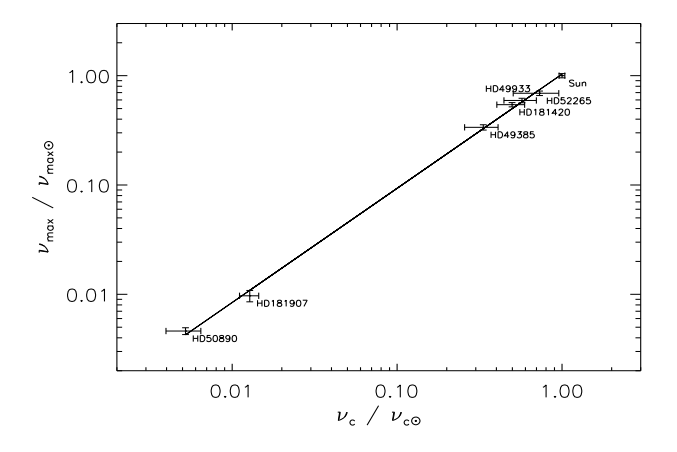


Fig. 1. Frequency of the maximum of oscillation power for the main- sequence and red-giant stars of Table 1 as a function of the frequency cut-off. All quantities are normalized to the solar values.

where ω is the angular frequency, W is the total work performed by the gas during one oscillation cycle, ξ is the displacement vector, and \mathcal{M} is the mode mass

$$\mathcal{M} = \int_0^M \frac{|\xi|^2}{|\xi_r(R)|^2} \, \mathrm{d}m \,. \tag{3}$$

 $\xi_r(R)$ corresponds to the radial displacement at the layer where the oscillations are measured, M is the total mass of the star.

For stochastically excited modes, the power injected into the modes is (e.g., Samadi & Goupil 2001; Belkacem et al. 2006)

$$P = \frac{1}{8M} (C_R^2 + C_S^2), \tag{4}$$

where C_R^2 and C_S^2 are the turbulent Reynolds stress and entropy contributions, respectively. We then introduce the height of the mode profile in the power spectrum, which is an observable, as (see e.g. Chaplin et al. 2005; Belkacem et al. 2006)

$$H = \frac{P}{2\eta^2 \mathcal{M}}.$$
 (5)

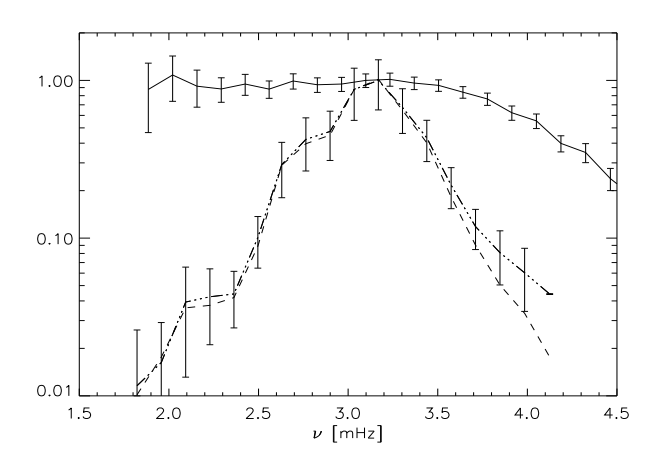


Fig. 2. Normalized $1/(2\Theta^2)$ (dashed-dots line), where $\Theta = \eta M$, and $\Pi = \mathcal{P} M$ (solid line) computed from solar seismic data from the GOLF instrument (Baudin et al. 2005). The normalized mode height (*H*) corresponds to the dashed line. All quantities are normalized to unity at the frequency of $\nu = \nu_{\text{max}}$. The associated mode masses are computed as described in Belkacem et al. (2006).

However, it is useful to express H in a form that does not explicitly depend on the mode mass (\mathcal{M}) . To this end, we note from Eqs. (2) and (4) that both the excitation P and the damping rate η are inversely proportional to the mode mass. Hence, to disentangle the effect of the driving and damping from the effect of mode mass, we introduce the quantities $\Pi = \mathcal{P} \mathcal{M}$ and $\Theta = \eta \mathcal{M}$, independent of mode masses. Then, using Eq. (5), the expression of the mode height becomes

$$H = \frac{\Pi}{2\Theta^2} \,. \tag{6}$$

Figure 2 displays the variations of H with mode frequency as well as its two contributions Π and $1/\Theta^2$. One can clearly distinguish a maximum for H near $\nu \simeq 3.2$ mHz that corresponds to the $\nu_{\rm max}$ frequency. Π remains roughly constant (efficient driving regime) except at high frequency beyond $\nu_{\rm max}$ which corresponds to the inefficient driving regime (see Samadi & Goupil 2001, for details). On the other hand $1/\Theta^2$ shows a sharp maximum and its variation clearly dominates over that of Π and controls the variation of H and the apparition of its maximum. We conclude that the maximum of H is determined by the minimum of H and corresponds to the plateau of the line widths. In other words, the depression (plateau) of the damping rates η is responsible for the presence of a maximum in the power spectrum, in agreement with Chaplin et al. (2008).

3.2. Origin of the depression of the damping rates

Balmforth (1992) mentioned that the depression of the solar damping rates originate from a destabilising effect in the superadiabatic layer. He also stressed that the plateau of the damping rates occurs when there is a resonance between the thermal time scale and the modal frequency.

Following these ideas, we use the MAD non-adiabatic pulsation code (Dupret 2002) for computing the solar damping rates. This code includes a time-dependent convection treatment (Grigahcène et al. 2005) different from that by Balmforth (1992). Nevertheless, we reach the same conclusion (see

Appendix A for details): the responsible for the destabilizing effect is the Lagrangian perturbation of entropy (δS) that exhibits a rapid variation mainly in the super-adiabatic layer as well as in the atmospheric layers (see Appendix A.2 and Fig. A.2).

To understand the origin of such an oscillation and illustrate the occurrence of the resonance, we consider the super-adiabatic layers and we examine the case of a highly non-adiabatic solution (see Pesnell 1984, for the case of a purely radiative envelope). We assume that Lagrangian perturbations of radiative and convective luminosities are dominated by perturbations of entropy (see Eq. (A.6) and Eq. (A.7)). This leads to a second-order equation for the **entropy perturbations** δS (Eq. (A.16), see Appendix. A.3 for the derivation). To obtain a more explicit solution for δS , we further employ the dimensional approximation $d\delta L/dr \sim \delta L/H_{P}$, so that

$$\frac{\mathrm{d}}{\mathrm{d}\ln T} \left(\frac{\delta S}{c_{\nu}} \right) + \lambda \left(\frac{\delta S}{c_{\nu}} \right) = 0, \quad \text{with} \quad \lambda = \mathcal{A} - i\,\mathcal{B}\,, \quad (7)$$

where $c_{\nu} = (\partial U/\partial T)_{\rho}$ with U the internal energy, \mathcal{A} and \mathcal{B} are defined by

$$\mathcal{A} = \left(\frac{L_c}{L}\psi \frac{\mathrm{d}\ln c_v}{\mathrm{d}\ln T} + \frac{L_R}{L}(4 - \kappa_T)\right) \left(1 + (\psi - 1)\frac{L_c}{L}\right)^{-1}$$

$$\mathcal{B} = Q\left[1 + (\psi - 1)\frac{L_c}{L}\right]^{-1}, \tag{8}$$

where $\kappa_T = (\partial \ln \kappa / \partial \ln T)_{\rho}$, L_c , and L_R are the convective and radiative luminosity respectively, T the temperature, ψ is defined by Eq. (A.8), and we have defined the ratio Q such as

$$Q = \omega \tau$$
, with $\tau^{-1} = \frac{L}{4\pi r^2 \rho c_v T H_p} = \tau_{\text{conv}}^{-1} + \tau_{\text{rad}}^{-1}$ (9)

with $\omega=2\pi\,\nu$, ν the modal frequency, τ a local thermal timescale, $\tau_{\rm rad}$ and $\tau_{\rm conv}$ the radiative and convective thermal timescales, respectively. From Eq. (A.12), the oscillatory part of the final solution is $(\delta S/c_{\nu}) \propto \exp\left[-i\int \mathcal{B}\,\mathrm{d}\ln T\right]$, which describes the oscillatory behaviour of entropy perturbations in the superadiabatic layers.

As discussed in Appendix B3 (Fig B2 top), all modes in the range of interest have a similar negative integrated work, W, at the bottom of the superadiabatic layer. This corresponds to a large damping at this level in the star. In the superadiabatic layers, the entropy's oscillatory behaviour controls the oscillating behavior of W. When the pulsation period and thus the wavelength of the entropy perturbations are too large ($Q \ll 1$), the destabilizing contribution has not grown enough; the cumulated work W increases too slowly. The net result at the surface is a large damping. When the period is too small $(Q \gg 1)$, the rapid oscillation of the entropy perturbation causes a rapid oscillation of W which increases and again decreases before reaching the surface and the net result at the surface is again a large damping. Those two limits correspond to low and high frequencies, i.e. to the two branches of $1/\Theta^2$ displayed in Fig. 2. A minimum damping is then obtained for a period neither too small nor too large i.e. $Q \simeq 1$ where the destabilizing contribution nearly but not quite compensates the strong damping of the layers below the super adiabatic layers.

The value of Q is illustrated in Fig. 3 for three modes. It confirms that the resonance $Q \simeq 1$ occurs in the super-adiabatic region for the mode with frequency $\nu \simeq \nu_{\rm max}$. Hence from the Q definition Eq. (9), one derives the resonance condition

$$v_{\text{max}} \simeq \frac{1}{2\pi \tau} \,. \tag{10}$$

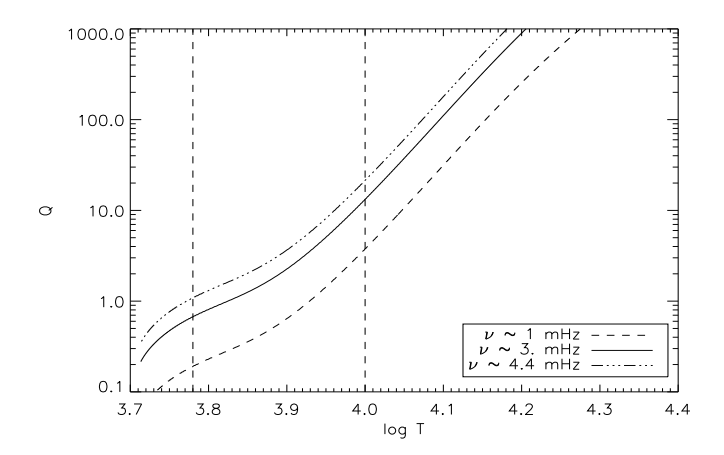


Fig. 3. Product Q (see Eq. (9)) versus the logarithm of the temperature for three values of the mode frequency, for a solar model described in Appendix A. Vertical dotted lines delimit the limits of super-adiabatic gradient (see Fig. A.2 bottom panel).

4. Derivation of the scaling law

We now turn to the relation between the thermal time-scale (τ) and the cut-off frequency. To this end, we use a grid of stellar models for masses between $M=1\,M_\odot$ and $M=1.4\,M_\odot$ from the ZAMS to the ascending **vertical** branch, typical of observed solar-like pulsators. The grid is obtained by using the stellar evolution code CESAM2k (Morel 1997; Morel & Lebreton 2008). The atmosphere is computed assuming a grey Eddington atmosphere. Convection is included according to Böhm-Vitense mixing-length (MLT) formalism. The mixing-length parameter is $\alpha=1.6$. The chemical composition follows Asplund et al. (2005), with an helium mass fraction of 0.2485. All quantities are evaluated at the maximum of the super-adibatic gradient, which corresponds to the maximum of δS (see Sect. 3.2) and the location of the resonance (see Eq. (10)).

From Fig. 4 (top), the relation between the thermal frequency $(1/\tau)$ and the cut-off frequency (ν_c) is close to linear but still shows a significant dispersion. More precisely, the relation between those two frequencies is approximatively linear and the dispersion is related to the dispersion in mass, in agreement with observations (e.g. Mosser et al. 2010). We then conclude that the observed relation between ν_{max} and ν_c is in fact the result of the resonance between ν_{max} and $1/\tau$, as well as the relation between $1/\tau$ and ν_c .

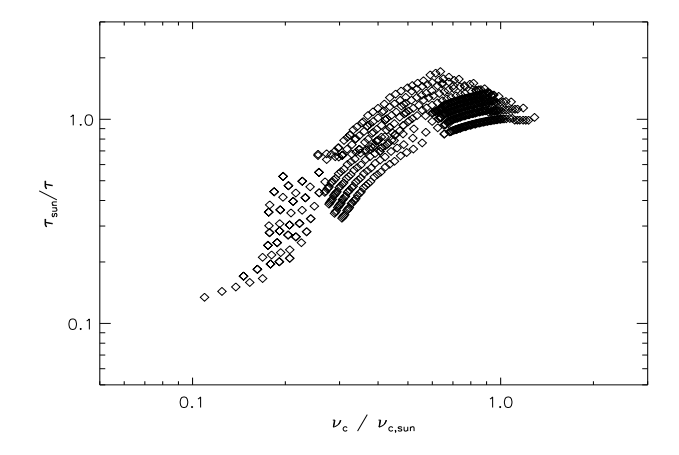
To go further, let us investigate the relation between $1/\tau$ and ν_c . First, Eq. (9) can be recast as

$$\frac{1}{\tau} = \frac{F_{\text{conv}}}{\rho c_v T H_p} \left[1 + \frac{F_{\text{rad}}}{F_{\text{conv}}} \right],\tag{11}$$

where $F_{\rm conv}$ and $F_{\rm rad}$ are the convective and radiative fluxes, respectively. The MLT solution for the convective flux and the convective rms velocity can be written (see Cox & Giuli 1968, for details)

$$F_{\text{conv}} = \frac{1}{2} \rho c_p \mathbf{v}_{\text{conv}} T \frac{\Lambda}{H_p} (\nabla - \nabla')$$
 (12)

$$\mathbf{v}_{\text{conv}} = \frac{\alpha c_{\text{s}} \Sigma^{1/2}}{2\sqrt{2} \Gamma_{1}^{1/2}} \left(\nabla - \nabla' \right)^{1/2} \tag{13}$$



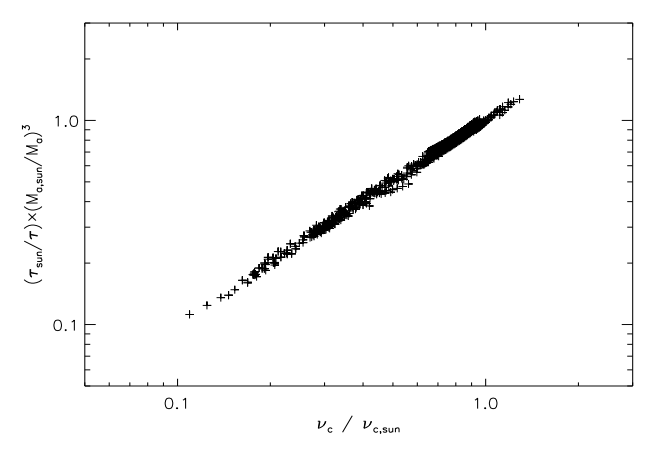


Fig. 4. Top: Thermal frequency $(1/\tau)$ computed from Eq. (9) versus the cut-off frequency computed following Eq. (1), normalized to the solar values, for models with masses ranging from $M = 1 M_{\odot}$ to $M = 1.4 M_{\odot}$ (with an increment of $0.05 M_{\odot}$) and from the ZAMS to the ascending vertical branch. **Bottom:** The same as for the top panel, except the thermal frequency is divided by the Mach number to the third versus the normalized cut-off frequency.

where $\Lambda = \alpha H_p$ is the mixing length, α the mixing-length parameter, $\nabla = (\mathrm{d} \ln T/\mathrm{d} \ln P)$, $\nabla' = (\mathrm{d} \ln T'/\mathrm{d} \ln P)$ the gradient of rising convective element, $\Sigma = (\partial \ln \rho/\partial \ln T)_{\mu,P}$, with μ the mean molecular weight, and $\Gamma_1 = (\partial \ln P/\partial \ln \rho)_{\mathrm{ad}}$. Now, by inserting Eq. (12) and Eq. (13) into Eq. (11), one obtains

$$\frac{1}{\tau} = 8 \left(\frac{\Gamma_1^2}{\chi_\rho \Sigma} \right) \left(\frac{\mathcal{M}_a^3}{\alpha} \right) \left(\frac{c_s}{2H_p} \right) \left[1 + \frac{F_{\text{rad}}}{F_{\text{conv}}} \right]$$
 (14)

where $\mathcal{M}_a = \mathbf{v}_{\text{conv}}/c_s$ the Mach number, and $\chi_\rho = (\partial \ln P/\partial \ln \rho)_T$.

We verified that for a given physic, the ratio $F_{\rm rad}/F_{\rm conv}$ is approximately the same for all the models considered in the superadiabatic layer. Hence, by use of Eq. (14) as well as the resonance condition (Eq. (10)), we conclude that

$$v_{\text{max}} \propto \frac{1}{\tau} \propto \left(\frac{\Gamma_1^2}{\chi_\rho \Sigma}\right) \left(\frac{\mathcal{M}_a^3}{\alpha}\right) v_{\text{c}},$$
 (15)

which is the observed scaling between v_{max} and v_{c} (see Fig. 1), since the thermodynamic quantities hardly vary.

Equation (15) describes the observed scaling between $\nu_{\rm max}$ and $\nu_{\rm c}$ (see Fig. 1) but also shows that most of the departure from the linear relationship between $1/\tau$ and $\nu_{\rm c}$ comes from the Mach number, as confirmed by Fig. 4 (bottom panel). We also point out that as shown by Fig. 4 and Fig. 1 for the main-sequence stars, the departure from the linear relationship is of the same order of magnitude as the uncertainties on the cut-off frequency. However, our grid of models is not suited for a proper comparison between the observations and the theoretical relation. This work is definitely desirable in the future.

5. Conclusion

We have addressed the issue of the physical reason for the existence of a scaling relation between $\nu_{\rm max}$ and $\nu_{\rm c}$. We have found that the depression of the damping rates determines $\nu_{\rm max}$ because there is a resonance between the local thermal time-scale in the super-adiabatic region and the modal period. This implies that $\nu_{\rm max}$ does not scale only with $\nu_{\rm c}$ but also with the ratio M_a^3/α . As pointed out in Sect. 1, the observed scaling between $\nu_{\rm max}$ and $\nu_{\rm c}$ is not obvious at first glance since the first frequency depends on the dynamical properties of the convective region while the second is a static property of the surface layers. The additional dependence the Mach number resolves this paradox.

This scaling relation is potentially a powerful probe to constraint the dynamical properties of the upper-most layers of solar-like pulsators through the ratio \mathcal{M}_a^3/α . Indeed, as shown in this paper, most of the dispersion in the $\nu_{\text{max}}-\nu_{\text{c}}$ scaling is related to the Mach number. The investigation of the ratio between ν_{max} and ν_{c} in main-sequence stars, subgiants, and red giants may give us statistical information on the evolution of the properties of turbulent convection from main-sequence to red giant stars, through for instance the mixing-length parameter. Indeed, a future work will consist in computing models, that correspond to the observations, and to make a comparison between the observed and theoretical dispersion from the linear relation between ν_{max} and

In other specific cases, for which stellar parameters are well known (e.g., in pulsating binaries) the relation between ν_{max} and ν_{c} could gives us directly the value of the Mach number in the upper-most convective layers.

Acknowledgements. K. B. gratefully acknowledges support from the CNES (Centre National dEtudes Spatiales) through a postdoctoral fellowship.

References

Asplund, M., Grevesse, N., & Sauval, A. J. 2005, in Astronomical Society of the Pacific Conference Series, Vol. 336, Cosmic Abundances as Records of Stellar Evolution and Nucleosynthesis, ed. T. G. Barnes III & F. N. Bash, 25-+

Ballot, J., Gizon, L., Samadi, R., et al. 2011, submitted to A&A

Balmforth, N. J. 1992, MNRAS, 255, 603

Balmforth, N. J. & Gough, D. O. 1990, ApJ, 362, 256

Barban, C., Deheuvels, S., Baudin, F., et al. 2009, A&A, 506, 51

Basu, S., Chaplin, W. J., & Elsworth, Y. 2010, Ap&SS, 328, 79

Baudin, F., Barban, C., Goupil, M., et al. 2011, et al., in preparation for A&A

Baudin, F., Samadi, R., Goupil, M.-J., et al. 2005, A&A, 433, 349

Bedding, T. R. & Kjeldsen, H. 2003, Publications of the Astronomical Society of Australia, 20, 203

Belkacem, K., Samadi, R., Goupil, M.-J., & Dupret, M.-A. 2008, A&A, 478, 163
Belkacem, K., Samadi, R., Goupil, M. J., Kupka, F., & Baudin, F. 2006, A&A, 460, 183

Benomar, O., Baudin, F., Campante, T. L., et al. 2009, A&A, 507, L13

Benomar, O., Baudin, F., Marques, J., et al. 2010, Astronomische Nachrichten, 331, 956

Brown, T. M., Gilliland, R. L., Noyes, R. W., & Ramsey, L. W. 1991, ApJ, 368, 599

Carrier, F., De Ridder, J., Baudin, F., et al. 2010, A&A, 509, A73+

Chaplin, W. J., Houdek, G., Appourchaux, T., et al. 2008, A&A, 485, 813

Chaplin, W. J., Houdek, G., Elsworth, Y., et al. 2005, MNRAS, 360, 859 Chaplin, W. J., Houdek, G., Karoff, C., Elsworth, Y., & New, R. 2009, A&A

Chaplin, W. J., Houdek, G., Karoff, C., Elsworth, Y., & New, R. 2009, A&A, 500, L21

Cox, J. P. & Giuli, R. T. 1968, Principles of stellar structure, ed. Cox, J. P. & Giuli, R. T.

Deheuvels, S., Bruntt, H., Michel, E., et al. 2010, A&A, 515, A87+

Dupret, M., Belkacem, K., Samadi, R., et al. 2009, A&A, 506, 57

Dupret, M.-A. 2002, Bull. Soc. Roy. Sc. Liège, 5-6, 249

Garcia, R. A., Palle, P. L., Turck-Chieze, S., et al. 1998, ApJ, 504, L51+

Grigahcène, A., Dupret, M.-A., Gabriel, M., Garrido, R., & Scuflaire, R. 2005, A&A, 434, 1055

Kallinger, T., Weiss, W. W., de Ridder, J., Hekker, S., & Barban, C. 2009, in Astronomical Society of the Pacific Conference Series, Vol. 404, Astronomical Society of the Pacific Conference Series, ed. B. Soonthornthum, S. Komonjinda, K. S. Cheng, & K. C. Leung, 307–+

Kjeldsen, H. & Bedding, T. R. 1995, A&A, 293, 87

Miglio, A., Montalbán, J., Baudin, F., et al. 2009, A&A, 503, L21

Morel, P. 1997, A&AS, 124, 597

Morel, P. & Lebreton, Y. 2008, Ap&SS, 316, 61

Mosser, B., Belkacem, K., Goupil, M., et al. 2010, A&A, 517, A22+

Pesnell, W. D. 1984, ApJ, 285, 778

Samadi, R. & Goupil, M. . 2001, A&A, 370, 136

Stello, D., Chaplin, W. J., Basu, S., Elsworth, Y., & Bedding, T. R. 2009a, MNRAS, 400, L80

Stello, D., Chaplin, W. J., Bruntt, H., et al. 2009b, ApJ, 700, 1589

Unno, W. 1967, PASJ, 19, 140

Appendix A: The *plateau* of the damping rates

A.1. Computation of the damping rates

Damping rates have been computed with the non-adiabatic pulsation code MAD (Dupret 2002). This code includes a time-dependent convection (TDC) treatment described in Grigahcène et al. (2005). This formulation involves a free parameter β which takes complex values and enters the perturbed energy equation. This parameter was introduced to prevent the occurence of non-physical spatial oscillations in the eigenfunctions. We use here the value $\beta = -0.55 - 1.7i$ which is calibrated so that resulting damping rates reproduce the variation of the solar damping rates η with frequency and more precisely the depression of the η profile (see Fig. A.1). Note that TDC is a local formulation of convection. This simplifies the theoretical description and is sufficient here as we seek for a qualitative understanding of the relation between the frequency location of the damping rate depression and the cut-off frequency. We stress that the above approximations do not influence qualitatively the conclusions.

This approach takes into account the role played by the variations of the convective flux, the turbulent pressure, and the dissipation rate of turbulent kinetic energy. Hence, the integral expression of the damping can be written as follows

$$\eta = \frac{1}{2 \,\omega \mathcal{M} \, |\xi_r(R)|^2} \int_0^M \mathcal{I} m \left[\frac{\delta \rho^*}{\rho} \left(\frac{\delta P_{\text{turb}}}{\rho} + (\Gamma_3 - 1) \, T \delta S \right) \right] dm \tag{A.1}$$

where $\xi_r(R)$ is the radial mode displacement at the photosphere, ω the mode frequency, ρ the mean density, $\Gamma_3 - 1 = (\partial \ln T/\partial \ln \rho)_S$, T the unperturbed temperature and the star denotes the complex conjugate. The symbol δ represents a Lagrangean perturbation: δS is the perturbation of specific entropy, $\delta \rho$ the density perturbation, δP_{turb} the perturbation of turbulent pressure. The quantity $\delta P_{\text{turb}}/\rho$ represents the contribution of turbulent pressure while the second term $(\Gamma_3 - 1)T\delta S$ includes the variations of radiative and convective fluxes as well as the dissipation rate of turbulent kinetic energy, as given by the energy conservation equation

$$i\sigma T\delta S = -\frac{\mathrm{d}\delta L_r}{\mathrm{d}m} - \frac{\mathrm{d}\delta L_c}{\mathrm{d}m} + \delta\epsilon_t$$
 (A.2)

with δL_r , δL_c being the perturbations of the radiative and convective fluxes respectively, $\delta \epsilon_t$ the perturbation of the dissipation rate of turbulent kinetic energy into heat, and $\sigma = \omega + i\eta$. Note that Eq. (A.2) is only valid for radial modes we are interested in.

A.2. Origin of the depression of the damping rates

The depression of the damping rates, located around $\nu \sim 3.5$ mHz (Fig.A.1), results from a subtle balance between the above contributions to the work integral. The cumulated work integral (regions where it increases outwards drive the oscillation and regions where it decreases outwards damp the oscillation) allows us to identify the processes that create this depression. Fig. A.2 (top) shows that mode damping results from stabilizing effects from inner layers at temperature greater than $\log T \sim 4$ destabilizing effects in the upper layers located in the super-adiabatic layers (*i.e.* between $\log T \sim 3.95$ and $\log T \sim 3.8$) and for high radial order modes again stabilizing effects from the very outer layers. Hence, the behavior of **the product** Θ **of the damping rates to the mode mass**, which is the integral appearing in Eq. (A.1), can then be described as follows: for modes with

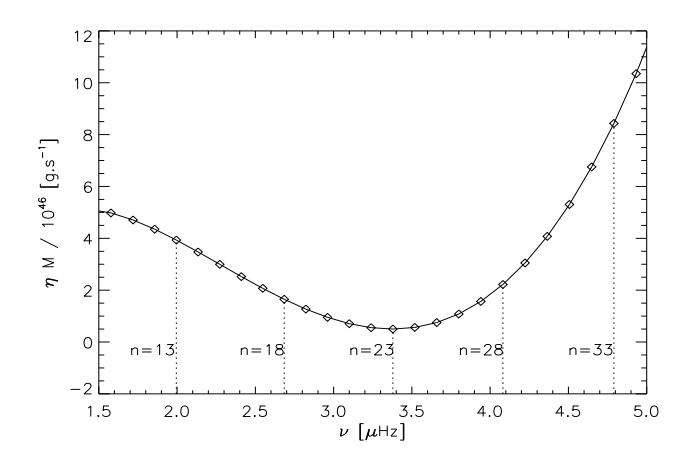


Fig. A.1. Product of the damping rates (η) times the mode mass (\mathcal{M}) versus mode frequency. The vertical dotted lines identify radial mode orders.

frequencies $\nu \leq \nu_{max}$ the higher the mode frequency the larger the contribution of the destabilizing region and Θ keeps on decreasing. For $\nu > \nu_{max}$, despite an increasing contribution of the superadiabatic boundary layers, atmospheric layers stabilize the modes resulting in an increase of Θ . At $\nu = \nu_{max}$, compensation is maximal giving rise to the minimum of Θ .

The physical cause of the destabilizing effects in the superadiabatic regions is revealed by Fig. A.2 (middle). The Lagrangian perturbation of entropy exhibits a rapid variation that occurs mainly in the super-adiabatic layer and in the atmospheric layers. As the frequency of the mode increases, the amplitude of this variation (which is a spatial oscillation as seen in the next section) also increases. The wavelenth of this spatial oscillation decreases with increasing frequency. This causes a similar behavior of the cumulated work.

A.3. Oscillation of entropy fluctuations

To understand the behaviour of δS in this region, let us first examine the fluctuations of radiative and convective luminosity appearing in the energy equation (Eq. (A.2)).

In the diffusion approximation, the fluctuations of radiative luminosity reads

$$\frac{\delta L_{\rm R}}{L_{\rm R}} = 2\frac{\xi_r}{r} + 3\frac{\delta T}{T} - \frac{\delta \kappa}{\kappa} - \frac{\delta \rho}{\rho} + \frac{{\rm d}\delta T/{\rm d}r}{{\rm d}T/{\rm d}r} - \frac{{\rm d}\xi_r}{{\rm d}r} \tag{A.3}$$

where ξ_r is the mode's radial displacement, δT the Lagrangian perturbation of temperature, $\delta \kappa$ the perturbation of opacity, and κ the opacity. By using the perturbed continuity equation Eq. (A.3), becomes, for radial modes,

$$\frac{\delta L_{\rm R}}{L_{\rm R}} = \frac{T}{{\rm d}T/{\rm d}r} \frac{{\rm d}}{{\rm d}r} \left(\frac{\delta T}{T}\right) + 4\frac{\delta T}{T} - \frac{\delta \kappa}{\kappa} \tag{A.4}$$

where we have neglected ξ_r/r compared to $\partial \xi_r/\partial r$. This assumption is valid for radial p modes (see Belkacem et al. 2008, for details). We further assume that, in the super-adiabatic region, perturbation of temperature fluctuations and opacity are dominated by entropy fluctuations, so that

$$\frac{\delta T}{T} \sim \frac{\delta S}{c_v}$$
 and $\frac{\delta \kappa}{\kappa} \sim \kappa_T \frac{\delta S}{c_v}$ (A.5)

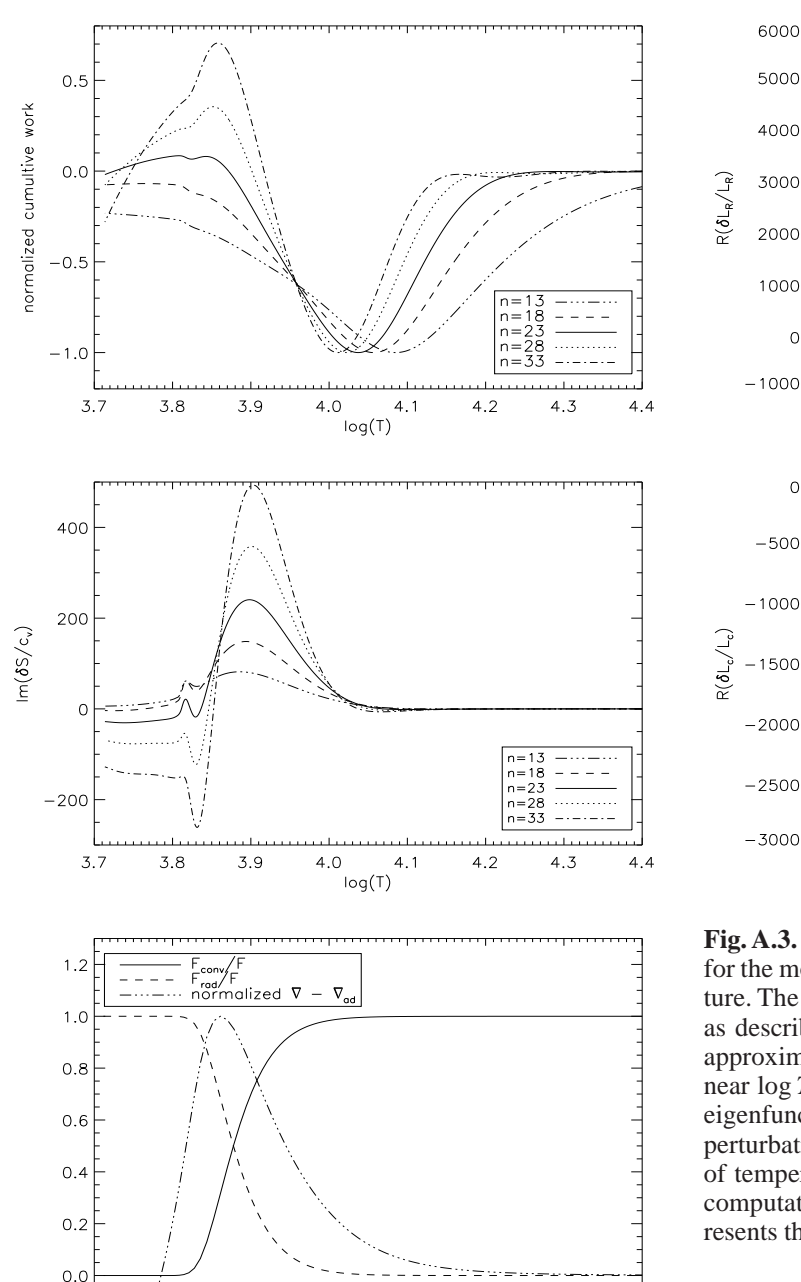


Fig. A.2. Top: Normalized cumulated work integral versus logarithm of temperature for five values of eigenfrequencies. These modes are emphasized in Fig. A.1. **Middle:** Imaginary part of the Lagrangian perturbation of entropy versus logarithm of temperature. **Bottom:** Normalized convective and radiative fluxes versus logarithm of temperature. The difference between the real and adiabatic gradient (∇) is also plotted and normalized to its maximum.

3.8

3.9

where $c_v = (\partial U/\partial T)_\rho$ with U the internal energy per unit mass, and $\kappa_T = (\partial \ln \kappa/\partial \ln T)_\rho$. Hence, inserting Eqs. (A.5) in Eq. (A.3) we obtain

$$\frac{\delta L_{\rm R}}{L_{\rm R}} \sim \frac{T}{{\rm d}T/{\rm d}r} \frac{{\rm d}}{{\rm d}r} \left(\frac{\delta S}{c_v}\right) + (4 - \kappa_T) \frac{\delta S}{c_v} \tag{A.6}$$

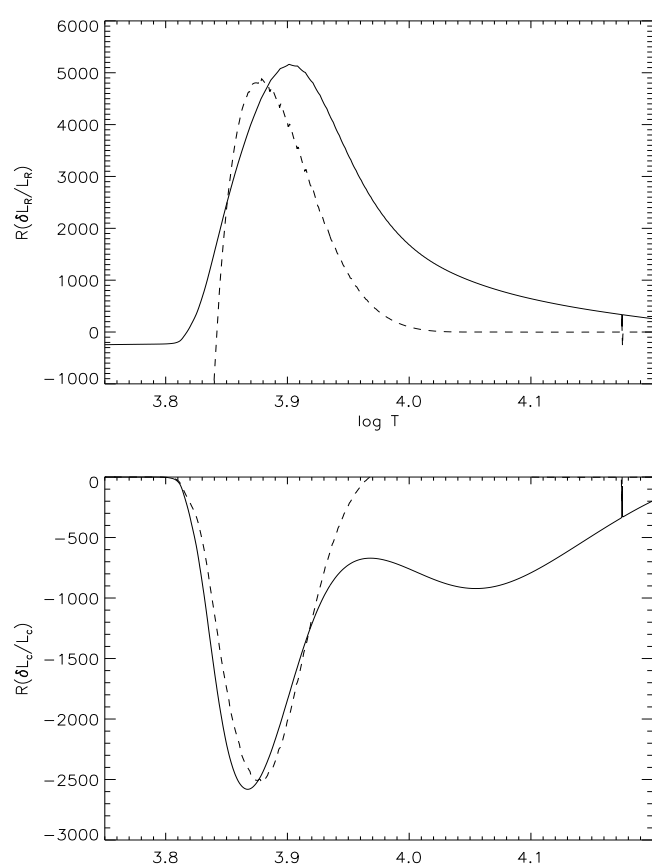


Fig. A.3. Top: Real part of the radiative luminosity perturbation for the mode of radial order n = 23 versus logarithm of temperature. The solid line represents the full non-adiabatic computation as described in Sect. A.1, while the dashed line represents the approximate expression given by Eq. (A.6). The rapid variation near $\log T = 4.17$ is the result of the presence of a node of the eigenfunction. **Bottom:** Real part of the convective luminosity perturbation for the mode of radial order n = 23 versus logarithm of temperature. The solid line represents the full non-adiabatic computation as described in Sect. A.1, while the dashed line represents the approximate expression given by Eq. (A.7).

The approximate expression Eq. (A.6), even if imperfect, captures the main behaviour of $\delta L_R/L_R$ in the superadiabatic boundary region, as shown by Fig. A.3 (top). Note that the disagreement observed in the inner layers in Fig. A.3 (top panel) is due to the approximation Eq. (A.5) since for those layers the density fluctuations are dominant. However, we are mainly interested in the super-adiabatic region (log T < 3.9) where Eq. (A.6) is sufficiently valid for our purpose.

We now turn to the Lagrangian perturbation of convective luminosity. It is dependent on the adopted time-dependent treatment of convection. Consistent with Sect. A.1, we use the formalism developed by Grigahcène et al. (2005). A good approximation of their Eq. (18) in the super-adiabatic layer, as shown by Fig. A.3 (bottom), is

$$\frac{\delta L_{\rm c}}{L_{\rm c}} \sim \psi \frac{{\rm d}\delta S}{{\rm d}S} = \psi \left[\frac{{\rm d}}{{\rm d}r} \left(\frac{\delta S}{c_{\nu}} \right) + \frac{{\rm d}\ln c_{\nu}}{{\rm d}r} \left(\frac{\delta S}{c_{\nu}} \right) \right] \frac{T}{{\rm d}T/{\rm d}r}, \quad (A.7)$$

with

$$\psi \backsim C \left(1 + \frac{((i+\beta)\sigma\tau_c + 2\omega_R\tau_c + 1)D}{B + ((i+\beta)\sigma\tau_c + 1)D} \right). \tag{A.8}$$

where τ_c is the life-time of convective elements, ω_R is the characteristic cooling frequency of the turbulent eddies, and

$$B = \frac{i\sigma\tau_c + \Lambda}{\Lambda},\tag{A.9}$$

$$C = \frac{\omega_R \tau_c + 1}{(i + \beta)\sigma \tau_c + \omega_R \tau_c + 1},$$
 (A.10)

$$D = \frac{C}{(\omega_R \tau_c + 1)} \,. \tag{A.11}$$

where $\Lambda = 8/3$ is a constant introduced by Unno (1967) to close the equation of motion describing convection, and ω_R is the characteristic cooling frequency of turbulent eddies due to radiative losses (see Eq. (C12) of Grigahcène et al. 2005).

We are now interested in obtaining the equation that qualitatively explains the oscillation observed in Fig. A.2 (middle panel). Hence, one has to exhibit in an analytical way the frequency dependence of the entropy fluctuations (δS). To this end, we will use two different assumptions. The first, and most immediate way is to assume that in the energy equation (Eq. (A.2)) $\mathrm{d}\delta L/\mathrm{d}r \sim \delta L/H_p$. This is a crude approximation, but which permits to immediately exhibit the role of the Q factor. Then using Eq. (A.6) and Eq. (A.7), one obtains

$$\frac{\mathrm{d}}{\mathrm{d} \ln T} \left(\frac{\delta S}{c_{\nu}} \right) + \lambda \left(\frac{\delta S}{c_{\nu}} \right) = 0, \quad \text{with} \quad \lambda = \mathcal{A} - i \mathcal{B}, \quad (A.12)$$

where \mathcal{A} and \mathcal{B} are defined by

$$\mathcal{A} = \left(\frac{L_c}{L}\psi \frac{\mathrm{d}\ln c_v}{\mathrm{d}\ln T} + \frac{L_R}{L}(4 - \kappa_T)\right) \left(1 + (\psi - 1)\frac{L_c}{L}\right)^{-1}$$

$$\mathcal{B} = Q\left[1 + (\psi - 1)\frac{L_c}{L}\right]^{-1}, \tag{A.13}$$

where we have defined the ratio Q as

$$Q = \omega \tau, \quad \text{with} \quad \tau^{-1} = \frac{L}{4\pi r^2 \rho c_v T H_p}$$
 (A.14)

with τ is a local thermal time-scale. Note that we have neglected the imaginary part of σ in Eq. (A.14). We stress that this thermal time-scale can be recast into

$$\tau^{-1} = \tau_{\text{conv}}^{-1} + \tau_{\text{rad}}^{-1} \tag{A.15}$$

where $\tau_{\rm conv}$ and $\tau_{\rm rad}$ are associated with the convective and radiative luminosities, respectively. From Eq. (A.12), the oscillatory part of the final solution is $(\delta S/c_{\rm v}) \propto \exp\left[-i\int \mathcal{B}\,\mathrm{d}\ln T\right]$, which explains the oscillatory behaviour of entropy perturbations in the super-adiabatic layers and its frequency dependence.

An alternative way to proceed is to use the energy equation (Eq. (A.2)) together with Eq. (A.6) and Eq. (A.7), one obtains the second order differential equation

$$\mathcal{F}\frac{\mathrm{d}^{2}}{\mathrm{d}\ln T^{2}}\left(\frac{\delta S}{c_{v}}\right) + \mathcal{G}\frac{\mathrm{d}}{\mathrm{d}\ln T}\left(\frac{\delta S}{c_{v}}\right) + \mathcal{H}\left(\frac{\delta S}{c_{v}}\right) = 0 \tag{A.16}$$

where

$$\mathcal{F} = 1 + (\psi - 1) \frac{L_c}{L}$$

$$\mathcal{K} = \frac{L_R}{L} (4 - \kappa_T) + \psi \frac{L_c}{L} \frac{\mathrm{d} \ln c_v}{\mathrm{d} \ln T}$$

$$\mathcal{G} = \frac{\mathrm{d}\mathcal{F}}{\mathrm{d} \ln T} + \mathcal{K}$$

$$\mathcal{H} = \frac{\mathrm{d}\mathcal{K}}{\mathrm{d} \ln T} - iQ \left(\frac{H_p}{H_T}\right)$$
(A.17)

where H_T is the temperature scale-height.

To derive an analytical solution of Eq. (A.16) is not trivial. Hence, further simplifications are needed. We then assume the coefficients $\mathcal{F}, \mathcal{G}, \mathcal{H}$ are constant. Assuming solutions of the form $(\delta S/c_{\nu}) \propto e^{k \ln T}$, one has the solutions for k

$$k_{1,2} = \frac{-\mathcal{G} \pm \left[\mathcal{G}^2 - 4\mathcal{H}\mathcal{F}\right]^{1/2}}{2\mathcal{F}} \tag{A.18}$$

At the maximum of the super-adiabatic gradient, the radiative luminosity dominates over the convective ones. Hence, we further neglect the ratio L_c/L compared with L_R/L . Eq. (A.18) then simplifies to

$$k_{1,2} = -\frac{1}{2} \left[\mathcal{G} \pm \left(\mathcal{G}^2 - 4 \frac{dG}{d \ln T} + 4iQ \left(\frac{H_p}{H_T} \right) \right)^{1/2} \right]$$
 (A.19)

From Eq. (A.19), one concludes that for $Q \ll 1$, k is real and δS does not oscillate. This corresponds to the limit of low-frequency modes for which both k and the imaginary part of δS are small, as confirmed by the full numerical computation presented in Fig. A.2 (middle panel). In contrast, for $Q \gg 1$ (i.e., for large frequencies) the imaginary part of the wavenumber increases as depicted by Fig. A.2 (middle panel).

Eventually, both methods to derive the frequency behaviour of δS converge toward the same conclusion, i.e. that the factor Q explains the oscillation of entropy fluctuations and its frequency dependence.